VALIDATION OF HYPERSPECTRAL CAMERA OPERATION WITH AN EXPERIMENTAL AIRCRAFT

Dennis D. Langer[1]*, Elizabeth F. Prentice*[2]*, Tor A. Johansen*[2]*, Asgeir J. Sørensen*[1]

Centre for Autonomous Marine Operations and Systems
[1]Department of Marine Technology
[2]Department of Engineering Cybernetics
Norwegian University of Science and Technology (NTNU), Trondheim, Norway

ABSTRACT

HYPSO-1 is a Small Satellite with a hyperspectral camera payload inside a six unit cubesat platform, launched january 2022. This paper describes how the operation of the same hyperspectral camera is validated by deployment on an experimental airplane, and how field trials are performed together with other remote sensing and in-situ agents. The payload is presented, in addition to how the operation was planned. The raw and radiance data are presented, and various practical aspects regarding implementation are discussed. Notwithstanding some minor issues, the procedures described were successfully used to gather valid data that can be used to infer properties of the imaged regions.

***Index Terms*—** Remote Sensing, Hyperspectral Imaging, Experimental Plane, Payload Operation, Field Test

1. INTRODUCTION

Imaging spectroscopy or Hyperspectal Imaging (HSI) is an interdisciplinary field related to remote sensing, which is concerned about creating an image in which every pixel contains dozens of bands uniformly sampled across usually the visible and infrared part of the electromagnetic spectrum. The result is a 3D dataset with two spatial dimensions and one spectral dimension [1].

With daylight returning from the arctic winter in spring, a number of factors contribute to a yearly ocean phytoplankton bloom, including meltwater runoff carrying nutrients, increasing temperatures, and increasing sunlight [2]. A yearly algae bloom happens typically late March to April in the seas around Norway. Bloom concentrations of phytoplankton can color the ocean surface, which can be detected and mapped using remote sensing. As opposed to multispectral imaging, hyperspectral imaging can enable a more detailed classification of phytoplankton blooms not limited to chlorophyll estimations, but for example distinguishing different taxa of phytoplankton like dinoflagellates or diatoms. [2, 3, 4].

In [5] the authors demonstrated the a method for HSI based on Commercial Off-The-Shelf (COTS) components and 3D printing, with a reduced cost to develop and manufacture do-it-yourself (DIY) HSI systems. This instrument design was based on S-mount optics and thus compact and light weight, being well suited for use on small drones. A larger instrument based on C-mount optics was then developed using the same principles to achieve higher throughput and Signal to Noise ratio (SNR) [6]. Its specifications were based on the HYPSO-1 satellite, [7], that carries a hyperspectral camera designed for observation of ocean color [8]. The satellite computer has onboard data processing capabilities to reduce data latency from capture to end user access for early detection of harmful algea blooms [9].

Multiple research groups at NTNU came together with the objective of detecting and monitoring parts of the 2021 spring algal bloom using remote sensing, in-situ agents and water sampling in Frohavet, off the coast of Trondheim, Norway. Every group had their individual goals of testing and verifying their sensor platforms. Five types of sensor-carrying platforms were used with three ways of measuring: An Autonomous Underwater Vehicle (AUV) and an Unmanned Surface Vehicle (USV) measuring among other quantities chlorophyll A concentration, manned boats taking water samples, a multicopter drone and a manned aircraft performing hyperspectral remote sensing with push broom cameras.

The objective of the manned aircraft mission was to test the process of integrating the payload into a new platform and to verify its operation.This work's scientific contribution is to demonstrate the successful commissioning and operation of the DIY hyperspectral camera payload [6, 8]. This paper presents similar work as [10, 11, 12] but with more focus on the operation.

This paper is structured as follows. First a technical overview of the setup is given in Section 2. Then, how the plane mission was planned is described and a recap of how it performed is given in Section 3. The data is presented in different stages of processing in Section 4. Finally, concluding remarks are given in the last Section 5.

2. OVERVIEW OF EXPERIMENTAL SET-UP

The hyperspectral camera was mounted on an RV-4 airplane licensed as experimental (Fig. 1). Experimental certification allows some modifications of the aircraft without losing the

This work was supported by the Research Council of Norway (RCN) through the MASSIVE project, grant number 270959, by the center of excellence AMOS, grant number 223254, and the Norwegian Space Agency contract UDF21014.

right to fly. The plane has two seats accommodating the pilot and the payload operator.

Fig. 1. Image of the RV-4 experimental airplane when it was landed at a nearby landing strip.

A single mechanical modification was done to the camera (Fig. 2) for mounting to the RV-4: The exchange of the component which is housing the slit behind the front objective with an aluminium block that can be mounted onto custom panels. The block was fixed to an aluminium hatch which replaced an identical hatch under one wing (Fig. 3). The camera was rigidly attached to the frame of the wing without damping or gimbal.

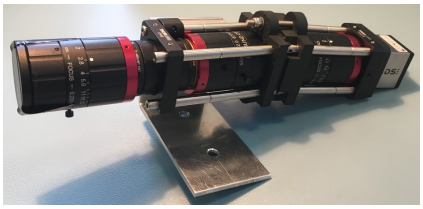

Fig. 2. The unmodified hyperspectral camera [6].

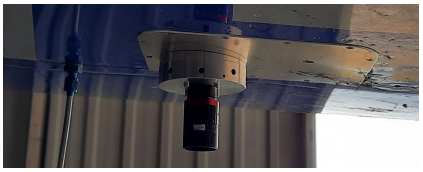

Fig. 3. The modified hyperspectral camera mounted under the left wing using custom aluminium parts.

In addition to the camera, the payload system consists of a stack of electrical components and a battery (Fig. 4). The stack is a modified version of the one presented in [13]. Modifications are to power delivery, embedded computer and software. Similarities to the HYPSO-1 payload are optics, image sensor, driver software and a similar but not identical Linux based operating system.

The embedded computer, a Nvidia Jetson TX2 is running DUNE [14] which is used for low level control and logging of camera data and other meta data sources. Notable meta data sources are an ADIS16490 Inertial Navigation Unit (IMU), an ublox NEO M8T Global Navigational Satellite System (GNSS) receiver and the flash signals from the hyperspectral camera. A Sentiboard [15] was used to assign a timestamp

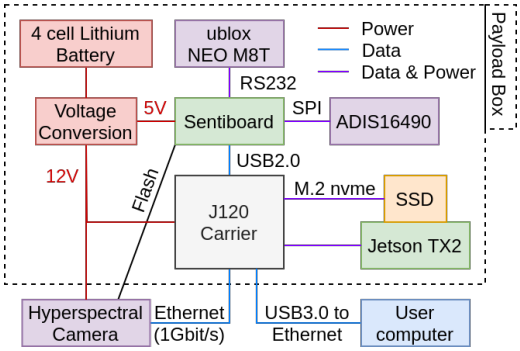

Fig. 4. The components of the hyperspectral camera payload. The box containing the component stack was strap-down mounted to the body of the plane.

to each data packet from these three data sources. The hyperspectral camera is connected to the stack with electric power (12V-24V), data (ethernet), and the flash signal for precise time recording of each image capture. Further specifications of the camera are in Table 1. The DUNE module for the hyperspectral camera supports control of parameters during recording, notably frame rate, exposure time, gain and spectral binning.

Table 1. Hyperspectral camera specifications

Sensitive spectral range	ca. 400-800nm
Bands after binning	ca. 120
Band pass	3.33 nm
Bitdepth	12 bit
Spatial pixels	500
Field of view	3.4 degrees

Radiometric and spectral calibration parameters were acquired by a calibration process using an integrating sphere and calibration light sources with argon and mercury gas similar as described in [16]. Care was taken to not perturb the camera much mechanically until it was mounted in the aircraft.

3. OPERATION OF AIRCRAFT AND PAYLOAD

Multiple iterations of testing were performed before the mission. They included software tests, lab tests, integration and functional tests in the plane hangar and finally flight tests.

Table 2. Data summary day 1

	Day 1			
	Flight 1		Flight 2	
	Rec. 1	Rec. 2	Rec. 1	Rec. 2
Duration	13m46s	18m44s	56m13s	23m39s
Lines	8380	15164	36990	28381
Data Size	1.96GiB	3.55GiB	8.67GiB	6.65GiB
Frame rate	10	10/15	10/15/20	20

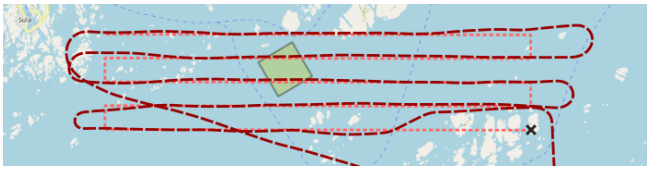

Fig. 5. Flight path of the fourth flight (dark, dashed) and planned paths (light, dotted). The green 1km x 1km square indicates the region of interest in which the other groups operated.

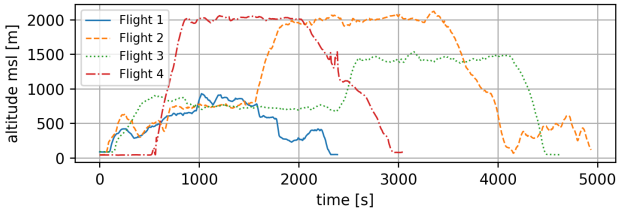

Fig. 6. Altitude mean-sea-level profile of all flights. Flight 1 was on lower and more varying altitude due to low cloud cover.

Several paths were planned using qGroundControl [17]. Long straight line paths were preferred to reduce geometric distortions in the unprocessed data due to rolling of the plane. The paths are passing over the in-situ mission area, which was a square of 1 km^2, shown in green in Fig. 5.

The planned paths were converted to a format compatible with SkyDemon [18]. Skydemon is a flight navigation app showing course and current location over flight maps. Skydemon was run on an Android tablet and was provided to the pilot for manual path following. No autopilot was used.

The nominal cruising speed of the RV-4 is about 70 m/s and the turning radius at that speed is 300m. The flights lines of the plan were made with a line spacing of 600m. The plane was not pressurized or temperature controlled, limiting the operable altitude. The location of clouds also constrained the area and altitude where the pilot could fly, as they should be avoided to prevent icing on the wings and protruding camera lens that degrade both camera and airplane performance.

Control software was written to provide indicators to the payload operator about image intensity and used for manual real time control of recording parameters. With a bitdepth of 12 bit, the maximum intensity value of one pixel on the image sensor is 4095. For good SNR and to prevent saturation, an average intensity value of half the maximum was targeted, leading to an SNR of about 150. A desired frame rate and exposure time to provide such an intensity was determined during the flight.

The RV-4 flew four times over two days, with two flights on each day. One flight path is shown in Fig. 5. The camera was continuously recording most of the flight time. An overview of the data from day 1 is shown in Table 2. Deviations from the ideal lawn mower pattern were in general due to manual piloting of the aircraft and in some cases due to clouds and bad GNSS fix. See Fig. 6 for altitude vs. time plots of the four flights.

4. RESULTS

Raw intensity values were converted to radiance using the radiometric calibration parameters. The spectral calibration parameters were used to compute wavelengths corresponding to the 242 bands. Radiometrically calibrated data is shown in Fig. 7. The spectra were generated by averaging a number of pixels belonging to the indicated class as determined by visual inspection.

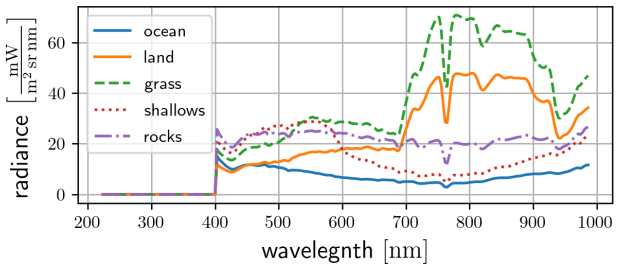

Fig. 7. Average spectral radiance of some surface classes that were recorded. The classes were averaged over a number of pixels: Ocean 894500 px. Land 31500 px. Grass 4588 px. Shallow water 10130 px. Rocks 188 px.

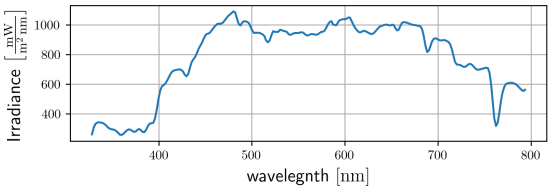

Fig. 8. In-situ solar irradiance spectrum

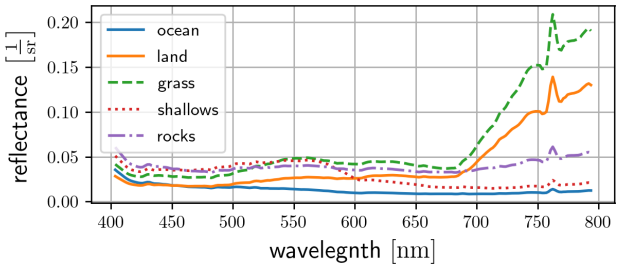

Fig. 9. Estimate of the remote sensing reflectance using the in-situ irradiance measurement. The inversion of the atmospheric oxygen absorption indicates issues with spectral or radiometric calibration.

A team operating from an island near the region of interest was taking solar irradiance measurements for calibration

of the remote sensing data (Fig. 7). No sign indicating significant presence of phytoplankton was seen in any ocean spectrum, a result which is confirmed by the in-situ data gathered by the USV and AUV's. This was likely due to bad weather throughout March and other external factors.

The SNR in the data is on average as high as expected, due to manual real time monitoring and control of recording parameters.

5. CONCLUSION

The operation of a DIY hyperspectral camera system as a remote sensing instrument was demonstrated. The system worked as expected and post-processing of the data demonstrated that spectral signatures were sufficiently detailed to discern different land cover classes. However, more data will need to be collected during an algal bloom event to fully assess the cameras performance for this application. Real time frame rate and exposure time control to worked well to obtain good SNR.

6. ACKNOWLEDGEMENTS

We thank Morten Raustein, Pål Kvaløy and Glenn Angell for assistance with the equipment and experiments.

7. REFERENCES

[1] H. M. Dierssen, S. G. Ackleson, et al., "Living up to the hype of hyperspectral aquatic remote sensing: Science, resources and outlook," *Frontiers in Environmental Science*, vol. 9, pp. 134, 2021.

[2] M. Winder and J. E. Cloern, "The annual cycles of phytoplankton biomass," *Philosophical Transactions of the Royal Society B: Biological Sciences*, vol. 365, no. 1555, pp. 3215–3226, 2010.

[3] D. Blondeau-Patissier, J. F. Gower, et al., "A review of ocean color remote sensing methods and statistical techniques for the detection, mapping and analysis of phytoplankton blooms in coastal and open oceans," *Progress in Oceanography*, vol. 123, pp. 123–144, 2014.

[4] S. Sathyendranath, Ed., *IOCCG (2014) Phytoplankton Functional Types from Space*, Number 15 in Reports of the International Ocean-Colour Coordinating Group. International Ocean-Colour Coordinating Group (IOCCG), Dartmouth, NS, Canada, 2014.

[5] F. Sigernes, M. Syrjäsuo, et al., "Do it yourself hyperspectral imager for handheld to airborne operations," *Opt. Express*, vol. 26, no. 5, pp. 6021–6035, Mar 2018.

[6] M. B. Henriksen, E. F. Prentice, et al., "Do-it-yourself vis/nir pushbroom hyperspectral imager with c-mount optics," *Opt. Continuum*, vol. 1, no. 2, pp. 427–441, Feb 2022.

[7] M. E. Grøtte, R. Birkeland, et al., "Ocean color hyperspectral remote sensing with high resolution and low latency–the HYPSO-1 cubesat mission," *IEEE Transactions on Geoscience and Remote Sensing*, pp. 1–19, 2021.

[8] E. F. Prentice, M. E. Grøtte, F. Sigernes, and T. A. Johansen, "Design of a hyperspectral imager using COTS optics for small satellite applications," in *International Conference on Space Optics — ICSO 2020*, B. Cugny, Z. Sodnik, and N. Karafolas, Eds. International Society for Optics and Photonics, 2021, vol. 11852, pp. 2154 – 2171, SPIE.

[9] B. Karlson, P. Andersen, et al., "Harmful algal blooms and their effects in coastal seas of northern europe," *Harmful Algae*, vol. 102, pp. 101989, 2021, Global Harmful Algal Bloom Status Reporting.

[10] B. de Goeij, G. Otter, et al., "First aircraft test results of a compact, low cost hyperspectral imager for earth observation from space," in *International Conference on Space Optics — ICSO 2016*, B. Cugny, N. Karafolas, and Z. Sodnik, Eds. International Society for Optics and Photonics, 2017, vol. 10562, pp. 465 – 475, SPIE.

[11] D. Turner, A. Lucieer, et al., "Pushbroom hyperspectral imaging from an unmanned aircraft system (uas) – geometric processingworkflow and accuracy assessment," *The International Archives of the Photogrammetry, Remote Sensing and Spatial Information Sciences*, vol. XLII-2/W6, pp. 379–384, 2017.

[12] J. Cristóbal, P. Graham, et al., "Airborne hyperspectral data acquisition and processing in the arctic: A pilot study using the hyspex imaging spectrometer for wetland mapping," *Remote Sensing*, vol. 13, no. 6, 2021.

[13] J. Fortuna and T. A. Johansen, "A lightweight payload for hyperspectral remote sensing using small UAVs," in *9th Workshop on Hyperspectral Image and Signal Processing: Evolution in Remote Sensing (WHISPERS)*, 2018, pp. 1–5.

[14] J. Pinto, P. S. Dias, et al., "The LSTS toolchain for networked vehicle systems," in *2013 MTS/IEEE OCEANS - Bergen*, 2013, pp. 1–9.

[15] S. M. Albrektsen and T. A. Johansen, "User-configurable timing and navigation for UAVs," *Sensors*, vol. 18, no. 8, 2018.

[16] M. B. Henriksen, E. F. Prentice, F. Sigernes, and T. A. Johansen, "Pre-launch calibration of the HYPSO-1 cubesat hyperspectral payload," in *Proc. IEEE Aerospace Conference*, 2022.

[17] "qgroundcontrol (v4.2.0)," (2021), Dronecode Project, [Online]. Available: http://qgroundcontrol.com/.

[18] "Skydemon," (2021), Divelements Limited, [Online]. Available: https://www.skydemon.aero/.